Modeling a layer 4-to-layer 2/3 module of a single column in rat neocortex: Interweaving *in vitro* and *in vivo* experimental observations

Leora Sarid*, Randy Bruno†, Bert Sakmann†‡, Idan Segev*‡§, and Dirk Feldmeyer¶

*Department of Neurobiology, Institute of Life Sciences, Jerusalem II-91904, Israel; §Interdisciplinary Center for Neural Computation, Hebrew University, Jerusalem II-91904, Israel; †Department of Cell Physiology, Max Planck Institute for Medical Research, D-69120 Heidelberg, Germany; and ¶Institute of Neuroscience and Biophysics, INB-3 Research Centre Jülich, D-52425 Jülich, Germany

Contributed by Bert Sakmann, August 22, 2007 (sent for review May 15, 2007)

We report a step in constructing an *in silico* model of a neocortical column, focusing on the synaptic connection between layer 4 (L4) spiny neurons and L2/3 pyramidal cells in rat barrel cortex. It is based first on a detailed morphological and functional characterization of synaptically connected pairs of L4–L2/3 neurons from *in vitro* recordings and second, on *in vivo* recordings of voltage responses of L2/3 pyramidal cells to current pulses and to whisker deflection. *In vitro* data and a detailed compartmental model of L2/3 pyramidal cells enabled us to extract their specific membrane resistivity (≈16,000 ohms·cm²) and capacitance (≈0.8 μF/cm²) and the spatial distribution of L4–L2/3 synaptic contacts. The average peak conductance per L4 synaptic contact is 0.26 nS for the α-amino-3-hydroxy-5-methyl-4-isoxazolepropionic acid and 0.2 nS for NMDA receptors. The *in vivo* voltage response for current steps was then used to calibrate the model for *in vivo* conditions in the Down state. Consequently, the effect of a single whisker deflection was modeled by converging, on average, 350 ± 20 L4 axons onto the modeled L2/3 pyramidal cell. Based on values of synaptic conductance, the spatial distribution of L4 synapses on L2/3 dendrites, and the average *in vivo* spiking probability of L4 spiny neurons, the model predicts that the feed-forward L4-L2/3 connection on its own does not fire the L2/3 neuron. With a broader distribution in the number of L4 neurons or with slight synchrony among them, the L2/3 model does spike with low probability.

barrel cortex | compartmental modeling | cortical column | L4-L2/3 synaptic connectivity | whisker deflection

Because of the unique relationship between the vibrissae and the barrel columns of the S1 cortex, where each column processes information primarily from one of the main facial whiskers (1), the somatosensory cortex of rodents is useful for studying sensory information processing within a single column and among neighboring cortical columns. The present experiment-based modeling study is an attempt to interweave *in vitro* and *in vivo* data measured from the barrel cortex. The aim is to begin to reconstruct the basic modules that serve as the building blocks of the cortical column.

The focus here is the simulation of the feed-forward excitatory connection between layer 4 (L4) spiny neurons and L2/3 pyramidal cells in the barrel cortex. The model is based first on the detailed morphology and physiology of L2/3 neurons, together with their dendritic location, the total number of synaptic contacts established by the axon of the L4 neuron on a single L2/3 neuron, and the properties of L4–L2/3 synaptic contacts, obtained from *in vitro* pair recordings of synaptically coupled neurons (2–4). Second, it is based on the *in vivo* current–voltage relationship (5) and on whole-cell recordings from L4 and L2/3 after whisker deflection (6).

The model does not meet the entire experimental finding during the process of interweaving *in vitro* and *in vivo* data. This mismatch enables one to suggest specific experiments for reconciling model and experiments. We therefore suggest that a systematic approach of modeling basic building blocks (connection "modules") of a column by combining *in vitro* pair recordings, anatomical reconstruction, and *in vivo* recordings from the respective projection and target cells of a connection might be a useful way to build a realistic model of an entire cortical column and to generate biologically realistic predictions.

Results

Passive Model for L2/3 Pyramidal Cells and Properties of L4–L2/3 Synaptic Contacts. Passive models were constructed for three fully reconstructed and physiologically characterized L4–L2/3 pairs, which include also the identification of the putative synapses and their dendritic locations. Our database contains 64 connected L4–L2/3 pairs. The dendritic arbors of three postsynaptic L2/3 neurons are shown in Fig. 1. The location of synaptic contacts formed by one presynaptic L4 spiny neuron on the L2/3 pyramidal cell is indicated by blue dots. The apical dendrite extended between 483 and 631 μm and the basal dendritic tree, between 129 and 224 μm. The average mean surface area of the dendritic arbor, including dendritic spines (see *Materials and Methods*), was calculated to be 20,651 μm^2.

Input resistance (R_{in}) was, on average, 77 megaohms (MΩ), and the membrane time constant was 13 ms (Fig. 1); these values are indeed within the range measured experimentally from a larger population of L2/3 pyramidal cells (72.7 ± 15.7 MΩ and 13.1 ± 1.7 ms, respectively; $n = 51$). Adjustment between model and experiments yielded average estimates for the membrane resistance (R_m) and membrane capacitance (C_m) of ≈16,000 Ωcm^2 and 0.8 $\mu F/cm^2$, respectively, assuming the axial resistance, $R_i = 150\ \Omega cm$ [supporting information (SI) Table 1], as found in other cortical neurons, and L5 pyramidal cells, hippocampal neurons, and cerebellar Purkinje cells (7–12). An example for the match between model response to current step and the experimental result is shown as Fig. 1 *Inset* (top left; green, model; red, experiments).

Time Course of a Unitary L4-to-L2/3 Excitatory Postsynaptic Potential (EPSP). An example of a L4-to-L2/3 unitary EPSP (from pair 111200A) is shown in Fig. 2*A* (gray line). The amplitude of this

Author contributions: B.S. and I.S. designed research; L.S., R.B., and D.F. performed research; L.S., R.B., and D.F. analyzed data; and L.S. wrote the paper.

The authors declare no conflict of interest.

Freely available online through the PNAS open access option.

Abbreviations: Ω, ohm; L*n*, layer *n*; EPSP, excitatory postsynaptic potential; AMPA, α-amino-3-hydroxy-5-methyl-4-isoxazolepropionic acid; AMPAR, AMPA receptor; NMDAR, NMDA receptor; EPSC, excitatory postsynaptic current; AP, action potential; c.v., coefficient of variation; PSTH, poststimulus time histogram.

‡To whom correspondence may be addressed. E-mail: sakmann@mpimf-heidelberg.mpg.de or idan@lobster.ls.huji.ac.il.

This article contains supporting information online at www.pnas.org/cgi/content/full/0707853104/DC1.

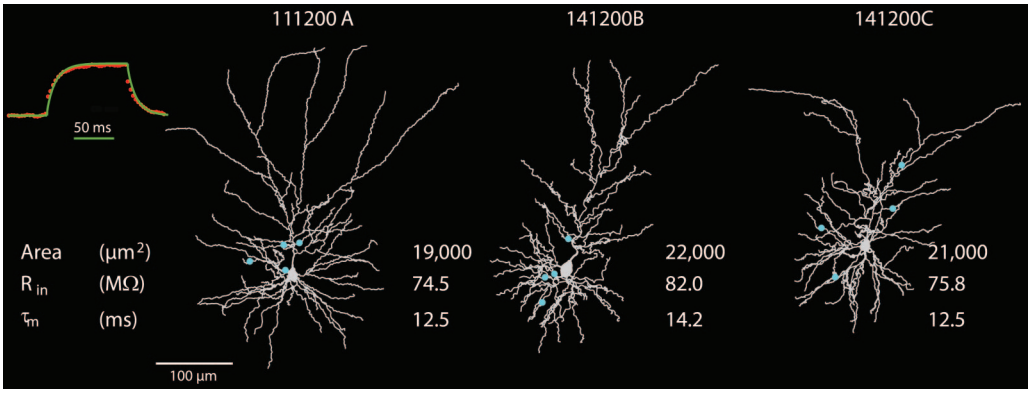

Fig. 1. Three reconstructed pyramidal L2/3 pyramidal cells from the barrel cortex. The dendrites of the pyramidal cells are in gray and, in each case, the putative synaptic contacts established with specific presynaptic L4 spiny neurons are marked by blue dots. The input resistance (R_{in}) and membrane time constant (τ_m) are extracted from experimental transients measured in these cells. The membrane area of the dendritic tree (including spines) is also denoted. (*Inset*) Voltage trace after a 100-ms current step in the passive model of cell 111200A (green continuous line) superimposed on the averaged and normalized experiment voltage traces measured in this same cell (red dotted line).

unitary EPSP is 0.66 mV, and the (20–80%) rise time is 0.9 ms; these values fall within the measured range of values (2). The generic Eqs. **1–5** provided in *SI Text* for the α-amino-3-hydroxy-5-methyl-4-isoxazolepropionic acid (AMPA) receptor (AMPAR) and NMDA receptor (NMDAR) were used to simultaneously fit both the target-cell EPSP in Fig. 2*A*, as well as the six traces for the NMDAR-mediated response in 1 mM extracellular Mg^{2+}, each measured at various membrane voltages, as shown in Fig. 2*B* (see *Materials and Methods*). The locations of the L4 synaptic contacts on the modeled L2/3 dendrites are as shown in Fig. 1. The black lines in Fig. 2 *A* and *B* depict the result of this fit. Similarly good fits between the experimental and model unitary EPSP were obtained for the other two connected neuron pairs depicted in Fig. 1 (not shown). Synaptic parameters obtained via this matching procedure are in SI Table 2.

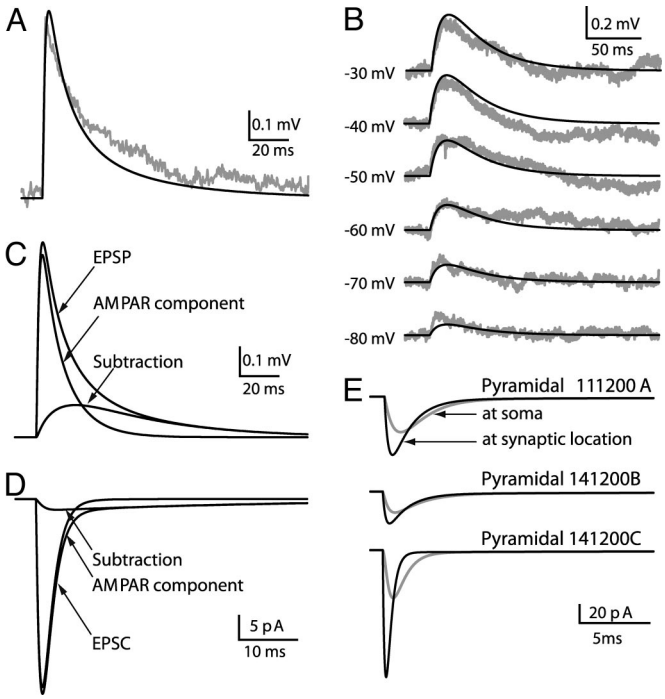

Fig. 2. Extracting synaptic parameters through fitting model to experiments. (*A*) An experimental average EPSP ($n = 39$) measured from the postsynaptic L2/3 neuron belonging to pair 111200A (gray line). The dark line is the model fit. (*B*) Isolated NMDAR-mediated voltage responses at different holding potentials (marked at left) recorded from another L2/3 pyramidal cell (gray lines). The model fits, which were based on morphology and locations of synaptic contacts for 111200A pair, are depicted by dark lines. (*C*) AMPAR and NMDAR components of the modeled EPSP in *A*. (*D*) AMPA- and NMDA-mediated currents under voltage–clamp (at −75 mV) in soma of modeled cell. (*E*) Space–clamp error in estimating synaptic current. Synaptic contacts were activated at their dendritic sites (blue points in Fig. 1), and voltage–clamp was applied at the soma (−75 mV). The measured synaptic current at the soma for the three cells modeled is shown in gray, and the case without space-clamp error is depicted by the corresponding black lines.

The maximal AMPAR conductance for the three target cells, on average, was 0.26 nS; the corresponding peak values for NMDAR conductance were 0.22 nS, on average. These values are within the range of values previously reported for the AMPAR and NMDAR conductances (13, 14). As expected, the time constant for the decay of the NMDAR-dependent response (τ_2) is ≈40-fold larger than for the AMPAR-dependent response (SI Table 2).

The contribution of the AMPAR and NMDAR components to the EPSP, as predicted by the model, is shown in Fig. 2*C*. For the three modeled cells, the average peak amplitude of the NMDAR channel-mediated voltage is 22% of the model EPSP, and the time integral of the NMDAR-mediated EPSP component, on average, was 52% of the total EPSP. The contribution of the AMPAR and NMDAR components to the current recorded at the soma of the modeled cell under voltage–clamp (at $V = -75$ mV) is shown in Fig. 2*D*. The unitary EPSCs at the soma for the three modeled cells are depicted by the gray lines in Fig. 2*E*. On average, the amplitude of the unitary somatic EPSC is −40 pA, varying between −24 and −55 pA. At the resting potential, the relative contribution of the NMDAR to the peak EPSC, on average, is 5.9%.

Fig. 2*E* also depicts the space–clamp error that results when determining unitary EPSCs from voltage–clamp measurements at the soma of the postsynaptic L2/3 neuron (15). The measured synaptic current at the soma for the three cells modeled is shown in gray. The dark lines show the postsynaptic current that would be generated when the same synaptic contacts are located at soma, where no space-clamp error is expected. The difference between the lines highlights the significant space-clamp error that is expected. For the upper two cells, the peak current under perfect voltage–clamp conditions is ≈1.5-fold larger than that in the experimental condition. In the third cell (lower traces), it is ≈2.5-fold larger. In this cell, the synaptic contacts are located more distally than in the other two cells (Fig. 1). Taking into

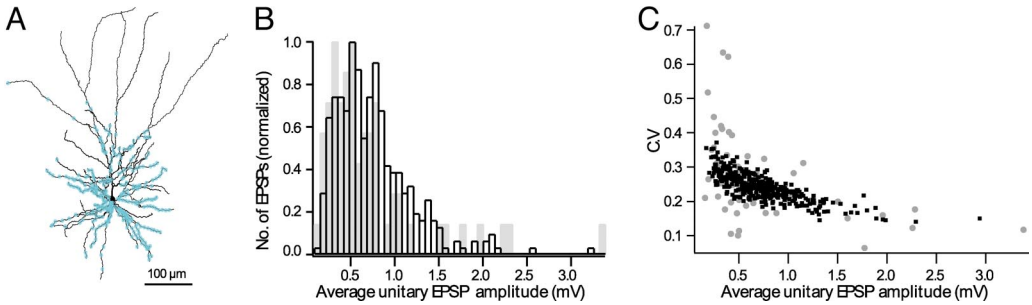

Fig. 3. EPSP histogram of L4 spiny neurons population converging onto a single L2/3 pyramidal cell. (*A*) Distribution of 1,575 L4–L2/3 synaptic contacts (from 350 axons) on the dendrites of a L2/3 modeled cell (see *Materials and Methods*). Each dot may represent more than one synaptic contact. (*B*) The average amplitude of the resultant 400 EPSPs from each axon is displayed (black squares) superimposed on the average unitary EPSP measured experimentally (gray squares). (*C*) The average c.v. plotted as a function of the EPSP peak amplitude (model in black, experiments in gray).

account the space-clamp error, the model predicts that the current generated at each individual synaptic contact ranges from 9 to 37 pA, which is in agreement with the range of 7–100 pA estimated for miniature excitatory postsynaptic current (mEPSC) in L2/3 pyramidal cells in the visual cortex (16).

Population of Unitary EPSPs at the L4–L2/3 Connection: Model vs. Experiments. Fitting the model to the experimental data for the L4-to-L2/3 pair recordings enabled us to estimate the properties of individual synaptic contacts (SI Table 2; Fig. 2). Next, we simulated the effect of APs in the ensemble of L4 spiny neurons that converge onto a single L2/3 pyramidal cell. We compared the modeling results to *in vivo* experimental data, i.e., the compound EPSPs, and evoked action potentials (APs) in L2/3 pyramidal cells.

We started by distributing the synaptic contacts established by the L4 axon on the appropriate dendritic domain ("innervation domain") of the postsynaptic L2/3 target neuron (3) and activating individual synapses (see *Materials and Methods*). We first asked whether the distribution of the modeled unitary EPSPs at the L4–L2/3 connection is similar to that found experimentally (see *Materials and Methods*). Specifically, average amplitude and coefficient of variation (c.v.) of unitary EPSPs were examined (Fig. 3).

On average, the amplitude of the model unitary EPSP was 0.73 ± 0.37 mV (Fig. 3*B*), and the c.v. was 0.24 ± 0.04 (Fig. 3*C*), which is in good agreement with the experimental data in which an average unitary EPSP amplitude of 0.7 ± 0.6 mV and a c.v. of 0.27 ± 0.12 were reported (2). This match between the EPSPs evoked by APs in a population of L4 neurons converging onto a specific dendritic domain of a single L2/3 neuron (rather than of individual L4-to-L2/3 connections) further strengthens the view that the model for the L4–L2/3 connection, including the dendritic domain for these synapses and the use of a lognormal distribution for the conductances of the receptors (see *Materials and Methods*), is "realistic." Therefore, this model was further used to explore how L2/3 pyramidal cells are expected to respond to a single whisker deflection when the input used was the average AP firing probabilities recorded *in vivo* from L4 spiny neurons, assuming that 350 ± 20 L4 neurons converge onto a single L2/3 neuron.

From *in Vitro* to *in Vivo*: An Important Modeling Leap. The interplay between the *in vitro* experiments and the corresponding model was critical for estimating the properties of L4–L2/3 synapses, including the conductances of their AMPA and NMDA components and the spatial distribution of this input on L2/3 dendrites. The modeling leap required for shifting from the *in vitro* conditions to the *in vivo* Down state condition (17) consists of three key steps. First, the input resistance should be reduced. In the *in vivo* conditions, R_{in} is ≈50% of the *in vitro* condition, probably because of the age (size) difference between the *in vitro* and *in vivo* experiments (18), yet the membrane time constant remains essentially the same in both conditions (5). Second, the strong anomalous rectification measured from the Down state in L2/3 cells (5, 19) should be captured. This nonlinearity was not an important factor for estimating the parameters of the relative small individual L4–L2/3 EPSPs measured from pair recordings. In contrast, it is important for modeling the *in vivo* conditions in which a large compound PSPs after whisker deflection is generated (and occasionally crossed spiking threshold). Third, the model should incorporate the very depolarized threshold for spiking, ≈30 mV above the resting potential found in both the *in vitro* and Down state *in vivo* conditions (5, 19).

Toward this end, cell 111200A, shown in Fig. 1, was used. First, we adjusted the passive membrane properties, and then we added membrane nonlinearities. By dividing R_m and multiplying C_m by a factor of 2.6, we took into account the likely increase in neuron size in the older rats measured *in vivo*, thus keeping the membrane time constant ≈10 ms and reducing R_{in} from 75 to 30 MΩ, as measured *in vivo* in the Down state (5). Our nonlinear model for the L2/3 pyramidal cell (SI Table 3) provided a very close fit of both the strong anomalous membrane rectification in the subthreshold regime and the very depolarized firing threshold as found experimentally [Fig. 4; compare experimental results; gray lines to model results (black lines)].

Simulation of the Response to a Whisker Deflection. Fig. 5 compares the distribution of experimentally measured compound PSPs after whisker deflection and the distributions predicted by the model (see *Materials and Methods*). The input to the modeled L2/3 neuron was based on the spiking probability of L4 neurons within the barrel (Fig. 5*A*, lower histogram), based on recordings of Brecht and Sakmann (20), and from additional recordings we performed from L4 neurons to have an adequately large data set (25 total L4 cells). Consequently, 130 axons of 350 (i.e., 460 synaptic contacts, assuming release probability of 0.79) were activated on average per whisker deflection (ranging between 96 and 166 axons), corresponding to 326–599 synaptic contacts). In the experiments, a broad distribution of compound PSPs was found, with average amplitude of 18 ± 10 mV (Fig. 5*B*). The rightmost bin (30 mV) is the contribution of mostly one cell (which is overrepresented with 149 traces of a total of 424 traces from a total of 20 cells) that tended to spike with high probability (0.53 APs per stimulus). With this cell included, the spiking probability is 0.23 APs per stimulus, whereas without this cell, the average amplitude of the compound PSPs was 17 ± 9 mV, and the corresponding firing probability was 0.06 APs per stimulus. The average amplitude of the compound EPSP in 1,000 simulations (Fig. 5*C*) is 12 ± 2.4 mV, with a much narrower

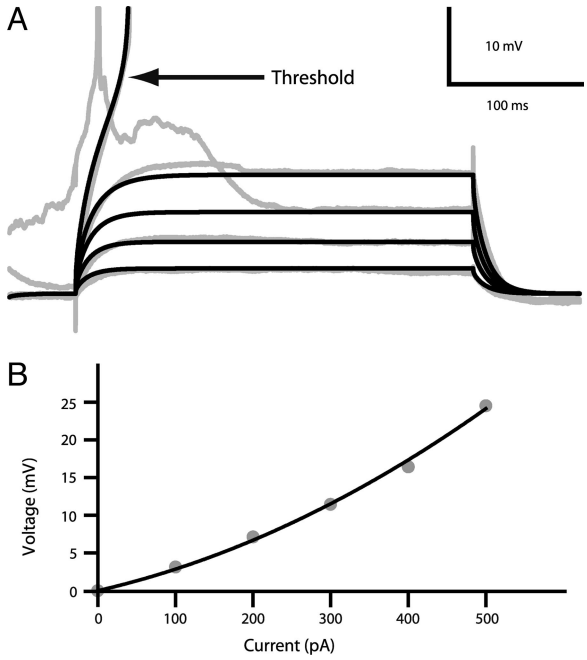

Fig. 4. Sub- and suprathreshold behavior for model compared with experiments. (*A*) Voltage recording from a L2/3 pyramidal cell recorded *in vivo* during 300-ms current steps, 100–500 pA (5) in gray compared with model response to the corresponding current step in black. (*B*) Steady-state V–I relationship shows anomalous rectification. Only Down state periods were analyzed (5) (gray dots). The black line is the second-order polynomial fit to the model I–V curve.

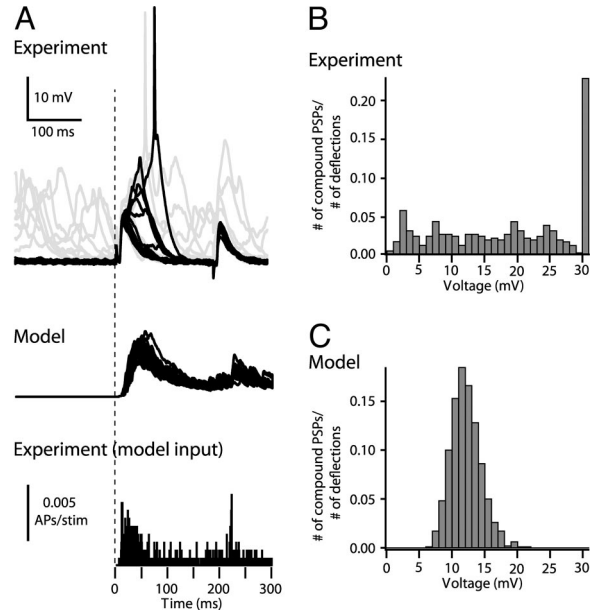

Fig. 5. Distribution of compound PSP amplitudes after whisker deflection, experiments vs. model. (*A*) Top trace. Records of 20 responses of a barrel-related L2/3 pyramidal cell to principal whisker deflection (courtesy of M. Brecht). Responses from the Down state are black (middle trace): 20 responses of the model-to-whisker deflection (lower trace). *In vivo* PSTH of L4 neuron after whisker deflection ($n = 25$) was used as an input for model (see *Materials and Methods*). The vertical dashed line denotes time of whisker deflection. (*B*) Experiments. (*C*) Model distribution of PSP amplitude from the Down state after whisker deflection.

distribution (ranging from 6 to 21 mV), as compared with the experimental results (Fig. 5 *A* and *B*). Importantly, the model does not fire APs, whereas in the experiment, the majority of L2/3 cells do fire with low probability (see *Discussion*).

To examine one possible source for the discrepancy between model and experiments, we conducted another set of simulations, in which the poststimulus time histogram (PSTH) of individual L4 cells (rather than of their average) was used as an input to activate L4–L2/3 synapses of the modeled L2/3 cell. The PSTHs of six individual cells (Fig. 6*A*, green) were used to activate the L2/3 modeled cell for 160 repetitions. Now the distribution of PSPs after whisker deflection is much broader than when the average PSTH (shown in Fig. 6*A*, blue) is used (compare Fig. 6*B*, green and blue), and L2/3 pyramidal cells fire occasionally (18% of the cases). This suggests that L4 neurons may not be randomly connected to L2/3 cells (21), but rather that subgroups of more excitable L4 cells exist (e.g., represented by the fourth PSTH from top in Fig. 6*A*) that may be responsible for the firing of some selected group of L2/3 cells (see *Discussion*).

Discussion

We propose here a step-by-step modular approach for modeling the cortical column by interlacing *in vitro* with *in vivo* data. The model enabled us first to estimate the passive and nonlinear membrane properties of L2/3 pyramidal cells, the properties of AMPA and NMDA components of the L4–L2/3 synapses, and the space-clamp error expected in estimating the properties of these synapses by voltage clamping the L2/3 pyramidal cell somata. The model also enabled us to predict that, based on current experimental data, L4 neurons alone do not fire L2/3 neurons after whisker deflection. The model provides several experimentally testable predictions for explaining the discrepancy between model and experiments.

The model of the postsynaptic L2/3 neuron as well as the putative location of the synaptic connections that give rise to an experimentally measured unitary EPSP enabled us to estimate synaptic parameters for both AMPAR and NMDAR for the L4–L2/3 connection with results agreeing with previous studies in neocortical and hippocampal pyramidal cells (12–14, 22). An

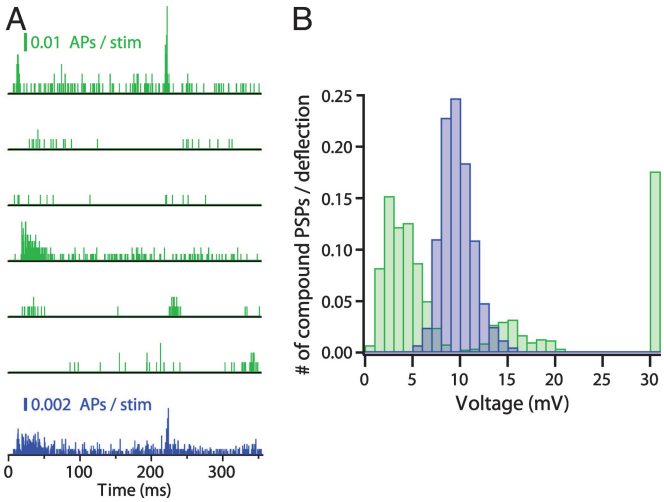

Fig. 6. Predicted distribution of the L2/3 compound PSPs when using either the average PSTH or that of individual L4 cells. (*A*) *In vivo* PSTH of six L4 neurons after whisker deflection (green) and the average PSTH (blue) (see *Materials and Methods*). (*B*) Composite PSP amplitude distribution after whisker deflection predicted by the model based on either individual PSTH shown in *A* (green histogram, $n = 1{,}000$) or the average PSTH (corresponding blue histogram, $n = 1{,}000$). Spiking is evoked for PSPs larger than 30 mV (rightmost bar).

important message from the model is that even for the electrically proximal dendritic domain (0.01λ–0.5λ) occupied by the L4-to-L2/3 connection, the space-clamp error in estimating synaptic parameters is substantial (between 160% and 300% error) and therefore must be corrected for.

The next step was to incorporate into the model *in vivo* measurements from L2/3 pyramidal cells in the Down state that show a decrease in input resistance as compared with the *in vitro* measurements (5, 6), marked anomalous rectification at the subthreshold regime, and very depolarized (≈30-mV) threshold for spiking. Incorporating membrane voltage-dependent ion channels into the passive model enabled us to capture the excitable properties measured *in vivo* (Fig. 4). Because specific experimental data are not yet available, the type of membrane ion channels and densities chosen (SI Table 3) do not necessarily represent faithfully the corresponding ion channels in these cells. However, the basic model predictions were robust when using other sets of excitable parameters (e.g., eliminating all dendritic ion channels but the A current; not shown), while preserving the target input resistance, the strong anomalous rectification, and the very depolarized threshold for spike generation as measured experimentally *in vivo*. Indeed, these *in vivo* phenomena both imply that a relatively large number of excitatory L4–L2/3 synapses are needed to cause an AP in the L2/3 neurons.

Having a realistic nonlinear model of an *in vivo* L2/3 neuron, we next used, as an input, the average firing probability (the PSTH) of L4 spiny neurons measured *in vivo* by using a whole-cell recording after passive whisker deflection (20). Assuming that ≈350 ± 20 L4 neurons converge onto a single L2/3 pyramidal cell (3), the model predicts that the average peak value for the compound PSPs is smaller than found experimentally, and that their amplitude distribution is much narrower. The consequence is that in L2/3 pyramidal cells, the model compound PSPs did not reach the voltage L2/3 threshold for spike firing (Fig. 5). In the experiments, these cells do fire (in 6% of the cases) to whisker stimulation.

This discrepancy between model and experiments is puzzling at first, because this model does not take into account inhibitory (feed-forward or lateral) connections that L2/3 neurons receive. However, neither does it take into consideration possible additional excitatory (thalamic or corticortical) inputs that L2/3 cells receive. L3 pyramidal cells, unlike L2 pyramidal cells, can receive direct thalamic input from the ventroposterior medial (VPM) nucleus of the thalamus, because their basal dendrites extend into L4, and because VPM afferents project into L3 (23, 24). Furthermore, paralemniscal pathways were not taken into account in this model, such as input to L2 from L5A (25) and L1 (26).

Other possibilities for explaining this discrepancy that require further experimental study are: (*i*) the existence of fine-scale subgroups of more excitable L4 spiny neurons (21) that may be responsible for the spiking of some selected group of L2/3 pyramidal cells (Fig. 6); (*ii*) the existence of synchrony in spiking of L4 neurons, similar to thalamic neurons driving L4 (27). Indeed, we found that even a small degree of synchrony among the L4 population increases the spiking probability of a L2/3 modeled L2/3 neuron (not shown). The above two possibilities are washed out when we use the average PSTH as an input. Recording simultaneously from many L4 neurons after whisker stimulation may unravel such specific intracortical spatiotemporal correlations. (*iii*) A broader distribution of the number of L4 axons converging onto a single L2/3 neuron. Indeed, increasing the standard deviation from 20 axons (around the mean of 350) to 100 results in a spiking probability of ≈7% in the modeled L2/3 neuron (not shown). (*iv*) Finally, it may be the case that only L2/3 pyramidal cells with large *in vivo* input resistance (i.e., 70 MΩ) may spike in response to whisker deflection. Measuring the input resistance of the cells and correlating it with their firing probability should help in examining this possibility.

To summarize, our modeling strategy is as follows: (*i*) start with what is known (at the spatial resolution of synapses and temporal resolution of spikes) and replicate the cortical column module of interest (L4–L2/3 excitatory connections in our case) as closely as possible; (*ii*) compare model behavior to *in vivo* experiments and, in turn, refine the model and perform additional experiments (see above) until a satisfactory match between the two is attained; and (*iii*) systematically reduce model complexity and generate successively more abstract models until a key function is lost, then study which are the crucial parameters that govern this function. Eventually, one hopes to derive a minimal mathematical description that captures the essence of the functioning of the whole column. With this method, one will be able to rigorously test, in terms of first principles, how the cortical substrate gives rise to cortical function.

Materials and Methods

Compartmental Modeling. Modeling was carried out by using the NEURON 5.8 simulator (28). 3D reconstructions of three synaptically connected L4–L2/3 pairs, in which the putative location of the synaptic connection is also available, were obtained by using a Neurolucida system (Microbrightfield, Colchester, VT) and converted to NEURON format. Dendritic sections were subdivided into compartments; each dendritic compartment is shorter than 20 μm. This yields between 742 and 871 compartments per neuron. The time step for simulations was 0.025 ms.

Passive Cable Model of L2/3 and L4-to-L2/3 Synaptic Properties. The specific passive R_m and C_m of L2/3 neurons were determined by matching model performance and *in vitro* experiments. For each reconstructed L2/3 pyramidal cell, we calculated the combination of R_i and R_m values that agrees with the experimental R_{in}. We found that the value of R_i = 150 Ωcm falls within the midrange for possible R_i values and, thus, R_i = 150 Ωcm was chosen (9). For this R_i value, R_m was determined individually for a given morphology, and it was then used for estimating C_m, so that $R_m \times C_m$ = the experimental membrane time constant, τ_m. Dendritic spines were incorporated globally into the modeled neuron as in ref. 29. The area of each dendritic spine was assumed to be 1 μm^2, and the spine density was 0.97 spine per micrometer of dendritic length (3).

The excitatory synapse between the L4-to-L2/3 connection is composed of both AMPAR and NMDAR components (2). We used the standard modeling approach for conductance-based synapses for both of these components (see *SI Text*). The target for model fitting was the unitary EPSPs that were recorded experimentally in each of the three morphologically reconstructed L2/3 pyramidal cells after AP stimulation in single presynaptic L4 spiny neurons together with six traces from another connected pair. In the latter case, the AMPARs were blocked by 10 μM 6-cyano-7-nitroquinoxaline-2,3-dione. NMDAR-mediated PSPs were recorded in the presence of 1 mM Mg^{2+}. In each case, synaptic inputs were activated at their putative locations (Fig. 1, blue dots). Using the MulrunFitter function in NEURON, we estimated the synaptic parameters for both AMPAR and NMDAR components that provide the best fit for the target experimental EPSPs.

Nonlinear Properties of L2/3 Neurons. L2/3 pyramidal cells exhibit strong anomalous rectification (5) as well as a high threshold for firing. The membrane ion channels that give rise to these nonlinearities were not fully characterized in these cells; we therefore incorporated into the passive skeleton of L2/3 neurons the most basic channel types that may give rise to these nonlinearities [I_{Na}, fast inactivating sodium current; I_{Kd}, delayed rec-

tifier (potassium) current; I_{Nap}, persistent sodium current; I_{AHP}, calcium-dependent potassium current; I_L, L-type calcium current; and I_A, A current]. We used NEURON′s MullrunFitter to fit the desired nonlinearities mentioned above (see details in *SI Text* and SI Table 3).

L4 Spiny Neurons Population Converging onto a Single L2/3 Pyramidal Cell. Between 300 and 400 L4 spiny neurons converge onto a single L2/3 pyramidal cell (3). Each L4 spiny neuron establishes ≈4.5 synaptic contacts on the target L2/3 pyramidal cell (2). Therefore, on average, 1,575 synaptic contacts are formed between L4 spiny neurons and a single L2/3 neuron. The distribution of synaptic input over the dendritic surface of a L2/3 neuron was taken from table 2 in Lübke *et al.* (3). To check the validity of this distribution, we activated individually 350 axons (each composed of four to five randomly chosen synaptic contacts of the total of 1,575). Each contact was activated 400 times, using the synaptic parameters that were found to fit the experimental unitary EPSP (SI Table 2). For each synapse activated, the maximal conductance for the AMPAR and NMDAR was chosen at random from a lognormal distribution, with a mean of 0.2 ± 0.095 nS for the AMPAR and 0.24 ± 0.05 nS for the NMDAR [these values were chosen so the relationship of unitary EPSP amplitudes to their c.v., as well as the distribution of amplitudes in the model, matches that of the experimental finding (2)]. The release probability at each synaptic contact in the model was 0.79 ± 0.04 (4).

Simulating Responses to Whisker Deflection. Whisker deflections that induced compound EPSPs and APs were simulated by activating L4 spiny neurons converging onto a single L2/3 pyramidal cell. In each simulation, the number of presynaptic L4 spiny neurons was randomly chosen from a normal distribution with a mean of 350 ± 20 (3). Axons were activated according to the average probability for APs (the average PSTH) in L4 spiny stellate neurons ($n = 19$), after whisker deflection, as reported in studies using whole-cell recordings *in vivo* (20) and from additional recordings of L4 cells ($n = 6$) that were done to confirm the original results and to enlarge our data set. In the 19 L4 neurons measured *in vivo*, the response to 20 repetitions of whisker deflection per cell was measured (20), whereas in the six additional recording neurons, there are 160 repetitions per cell so that the PSTH of these six neurons could be used individually as an input for the model (Fig. 6). The simulated compound PSPs were compared with the experimental PSPs, measured from the Down state in 16 L2/3 pyramidal cells (6) and from four additional recordings of L2/3 cells.

We thank Michael Brecht (Bernstein Center for Computational Neuroscience, Humboldt University Berlin, Berlin, Germany), Jack Waters (Northwestern University Interdepartmental Neuroscience Program, Chicago, IL), Fritjof Helmchen (Brain Research Institute, Department of Neurophysiology, Zurich, Switzerland), and Christiaan De Kock (Department of Cell Physiology, Max Planck Institute for Medical Research, Heidelberg, Germany) for making their data so generously available to us. We also thank Arnd Roth for assistance along the course of this study. This work is supported by the Israeli Science Foundation and the Volkswagen Foundation.

1. Simons DJ (1978) *J Neurophysiol* 41:798–820.
2. Feldmeyer D, Lübke J, Silver RA, Sakmann B (2002) *J Physiol* 538:803–822.
3. Lübke J, Roth A, Feldmeyer D, Sakmann B (2003) *Cereb Cortex* 13:1051–1063.
4. Silver RA, Lübke J, Sakmann B, Feldmeyer D (2003) *Science* 302:1981–1984.
5. Waters J, Helmchen F (2006) *J Neurosci* 26:8267–8277.
6. Brecht M, Roth A, Sakmann B (2003) *J Physiol* 553:243–265.
7. Stuart G, Spruston N (1998) *J Neurosci* 18:3501–3510.
8. Gentet LJ, Stuart GJ, Clements JD (2000) *Biophys J* 79:314–320.
9. Trevelyan AJ, Jack J (2002) *J Physiol* 539:623–636.
10. Roth A, Hausser M (2001) *J Physiol* 535:445–472.
11. Clements JD, Redman SJ (1989) *J Physiol* 409:63–87.
12. Major G, Larkman AU, Jonas P, Sakmann B, Jack JJ (1994) *J Neurosci* 14:4613–4638.
13. McBain C, Dingledine R (1992) *J Neurophysiol* 68:16–27.
14. Spruston N, Jonas P, Sakmann B (1995) *J Physiol* 482:325–352.
15. Rall W, Segev I (1985) in *Voltage and Patch Clamping with Microelectrodes*, eds Smith TG, Lecar H, Redman SJ, Gage PW (Am Physiol Soc, Bethesda, MD), pp 191–215.
16. Myme CI, Sugino K, Turrigiano GG, Nelson SB (2003) *J Neurophysiol* 90:771–779.
17. Cowan RL, Wilson CJ (1994) *J Neurophysiol* 71:17–32.
18. Zhu JJ (2000) *J Physiol* 526:571–587.
19. Feldmeyer D, Lübke J, Sakmann B (2006) *J Physiol* 575:583–602.
20. Brecht M, Sakmann B (2002) *J Physiol* 543:49–70.
21. Yoshimura Y, Dantzker JL, Callaway EM (2005) *Nature* 433:868–873.
22. Burgard EC, Hablitz JJ (1993) *J Neurophysiol* 70:1841–1852.
23. Arnold PB, Li CX, Waters RS (2001) *Exp Brain Res* 136:152–168.
24. Jensen KF, Killackey HP (1987) *J Neurosci* 7:3544–3553.
25. Shepherd GM, Stepanyants A, Bureau I, Chklovskii D, Svoboda K (2005) *Nat Neurosci* 8:782–790.
26. Cauller LJ, Connors BW (1994) *J Neurosci* 14:751–762.
27. Bruno RM, Sakmann B (2006) *Science* 312:1622–1627.
28. Hines ML, Carnevale NT (1997) *Neural Comput* 9:1179–1209.
29. Stratford AU, Mason A, Larkmann AU, Major G, Jack JJB (1989) in *The Computing Neuron*, eds Durbin R, Miall C, Mitchson G (Addison–Wesley, Wokingham, UK), pp 296–321.